Minimization of the Plane-Wave Scattering Contribution of Inverted-Y Strut Tripods to the Noise Temperature of Reflector Antennas

Fernando J. S. Moreira, *Student Member, IEEE*, Aluizio Prata, Jr., *Member, IEEE*, and Michael A. Thorburn, *Senior Member, IEEE*

Abstract—**This work is concerned with determining the metallic strut cross section of inverted-Y tripods to minimize the plane-wave scattering contribution to the noise temperature of ground-station reflector antennas and radio telescopes. This is accomplished by numerically optimizing the cross section for minimum ground-noise pickup over the antenna elevation-angle operation range. Advantage is taken of the fact that although the struts' cross-section perimeter can be comparable to the operation wavelength, their electrical lengths are usually long. This allows the struts' scattering characteristics to be determined by solving standard two-dimensional field integral equations. This work concentrates on the top strut of an inverted-Y configuration since it is responsible for the dominant ground noise pickup associated with the plane-wave scattering. Numerical simulations are presented to substantiate this fact and a simple and convenient broadband closed-form representation for the minimum-noise top-strut cross section is derived and tested.**

I. Introduction

AXIALLY-SYMMETRIC ground-station reflector-antenna systems are widely used in numerous applications such as deep-space links, satellite communications, radio astronomy, and radar. In the majority of these applications, the system has either one or two reflectors, and in both cases the antenna entrance aperture is partially obstructed by the feed (single reflector), feed and subreflector (dual reflector), and their respective supporting structures (struts). This blockage decreases the overall antenna gain, increases the sidelobe and cross-polarization levels, and increases the antenna noise temperature. The electrical impact of the struts on the reflector-antenna performance has been investigated by several authors. Although considerably more emphasis has been placed on gain-loss and co- and cross-polarization radiation pattern effects [1]–[3], recently several authors have also been specifically concerned with the strut contribution to the antenna noise temperature [4]–[7]. Of particular interest is the minimization of the noise-temperature dependence on the antenna orientation, a critical effect in radio-astronomy measurements of the cosmic microwave background-radiation anisotropy [6].

The equivalent antenna noise temperature T_A is primarily caused by the environment thermal radiation, which is proportional to the environment absolute temperature T_e. Invoking the reciprocity between the receive and transmit antenna operation modes, the antenna noise temperature can then be regarded as being produced by the transmitting antenna power radiated toward the environment (sky and ground). Hence, the antenna noise temperature is intrinsically dependent on the antenna orientation and radiation pattern. It is known that the blockage caused by the antenna struts produces relatively large conical sidelobes that cross the radiation-pattern main beam. These sidelobes are the radiation cones (strut cones [2]) generated when the struts scatter the quasi-plane wave that leaves the main reflector. Hence, depending on the antenna orientation, part of these strut cones may illuminate the relatively warm ground ($T_e \approx 300\,K$) in the near field, picking up more thermal noise than if they illuminated the sky ($T_e \approx 5\,K$, including high-elevation angle ideal atmospheric attenuation).

There are other important effects that contribute to the antenna ground-noise pickup besides the strut cones associated with the plane-wave scattering. For instance, the quasi-spherical waves radiated by the feed and by the subreflector (when it is present) are also scattered by the struts and may illuminate the ground. In general, however, the feed energy is highly tapered when it illuminates the struts, and the associated noise pickup can be neglected. Furthermore, for physically-large shaped dual-reflector antennas designed for optimum gain and noise performance, the struts are commonly attached well inside the main-reflector surface. Due to this, most of the subreflector radiation scattered by the struts illuminates the main reflector, and hence, does not go to ground. For these reasons, the strut spherical-wave scattering is not considered in this work. There is also the contribution of the feed and subreflector spillover, but this effect is outside the scope of the present work.

The objective of this work is to minimize the strut-cone power density produced by the plane-wave scattering that illuminates the relatively warm ground. Simple geometric considerations indicate that the struts located on the main-reflector upper half will scatter substantially more power density toward the ground than the ones on the lower half.

Manuscript received July 12, 1995. This work was supported by the Jet Propulsion Laboratory, California Institute of Technology, Pasadena, under a contract with the National Aeronautics and Space Administration. F. J. S. Moreira was supported by a scholarship from the Brazilian Agency CNPq.

F. J. S. Moreira and A. Prata, Jr. are with the Department of Electrical Engineering–Electrophysics, University of Southern California, Los Angeles, CA 90089-0271 USA.

M. A. Thorburn is with the Jet Propulsion Laboratory, California Institute of Technology, Pasadena, CA 91109-8099 USA.

Publisher Item Identifier S 0018-926X(96)02632-4.

For this reason, only an inverted-Y strut configuration is considered here—the inverted-Y geometry has the minimum number of struts (i.e., one) located on the top half of the antenna. In the next section, the contribution of the strut radiation cone to the antenna temperature is determined. In Section III, this result is used to numerically optimize the top-strut cross section to further reduce its plane-wave scattering toward ground. Based on the optimized results obtained in Section IV, a broadband closed-form representation is derived for the optimum top-strut cross section.

The reduction of the strut contribution to the antenna noise temperature can also be accomplished by introducing corrugations at the strut surface [8] or by covering it with a dielectric layer [9], [10]. However, the present work is concerned with optimizing the cross-section geometry of an all-metallic strut. Retrofitting an existing antenna with an optimum-profile strut may be a less expensive alternative to reduce the antenna noise temperature.

II. Strut-Cone Noise-Temperature Contribution

As mentioned above, the objective of this work is to reduce the strut-cone power scattered toward the relatively warm ground. A rigorous calculation of the strut-scattered field is somewhat involved since it must take into account the actual strut geometry (e.g., truss configuration), its relative location on the antenna, the spherical- and plane-wave scattering mechanisms, multiple reflections in the antenna system, etc. However, the problem can be rendered more tractable using a simplified yet accurate model. This model considers only the plane-wave scattering and, for the purpose of determining the induced surface-current densities, considers the strut as an infinitely-long perfect electric conducting cylinder of arbitrary cross section. The finite strut length is taken into account afterwards by truncating the strut to a finite length once its surface currents are known. Although this model is approximate, it is capable of modeling struts (with good accuracy) not constructed of separate members (e.g., truss struts).

An infinitely-long perfect electric conductor illuminated by a plane wave scatters an electromagnetic field that can be represented by cones of rays (strut cones) propagating away from the strut [7], as illustrated on Fig. 1. The strut-cone semi-angle θ_c is identical to that between the incident plane-wave Poynting vector and the cylinder axis. At large distances from the cylinder axis the scattered-wave power density is given by

$$S_s^E(\vec{\rho}) = \frac{1}{2\eta_o}\,\vec{E}_s \cdot \vec{E}_s^* = \frac{1}{2\eta_o}\,\frac{|E_{zs}(\vec{\rho})|^2}{\sin^2\theta_c} \tag{1}$$

$$S_s^H(\vec{\rho}) = \frac{\eta_o}{2}\,\vec{H}_s \cdot \vec{H}_s^* = \frac{\eta_o}{2}\,\frac{|H_{zs}(\vec{\rho})|^2}{\sin^2\theta_c} \tag{2}$$

where the superscripts E and H denote the E (no magnetic field along the cylinder axis) and H (no electric field along the cylinder axis) polarizations, respectively, η_o is the free-space wave impedance, $\vec{\rho}$ is the usual cylindrical coordinate position vector (the z-axis is assumed along the cylinder axis), and E_{zs} and H_{zs} are the scattered electric and magnetic field $\hat{z}$-components, respectively. E_{zs} and H_{zs} can be obtained by solving the two-dimensional electric and magnetic field integral equations using method of moments (MoM) techniques [11]. Throughout this work a plane wave with a 1 V/m electric-field amplitude has always been used to illuminate the struts.

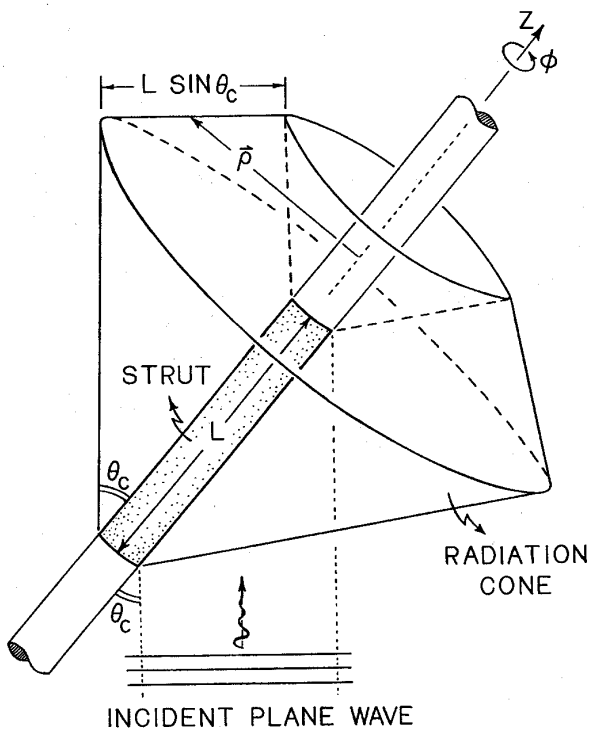

Fig. 1. Finite-length strut-scattering parameters.

Once the infinite-length strut currents are known and their radiated field determined, the finite length of practical struts is taken into account. This can be done recalling that a long finite-length strut still radiates, for near-zone observation points in the θ_c-direction, scattered rays with the same power density as the infinite-length strut [4]. Note that in the far-zone, the finite-length strut produces a radiation pattern very different from the infinite-length one [2], [3]. However, for the problem at hand we only need to be concerned with the near-zone pattern of the finite-length strut. Hence, the power ΔP_s scattered by the finite-length strut inside a sector of angular width $\Delta\phi$ is

$$\Delta P_s(\phi) = S_s(\vec{\rho})\;\; L\;\rho\;\sin\theta_c\;\;\Delta\phi \tag{3}$$

where S_s is given by (1) and (2), depending on the wave polarization, L is the strut length, and ρ and ϕ are the cylindrical coordinates shown in Fig. 1. The contribution of ΔP_s to the antenna noise temperature is given by

$$\Delta T(\theta_{el},\phi) = \frac{T_e(\theta_{el},\phi)}{P_{in}}\;\;\Delta P_s(\phi) \tag{4}$$

where P_{in} is the total power radiated by the antenna and T_e is the environment noise temperature. T_e is a function of the antenna elevation angle θ_{el} and the strut-fixed azimuth angle ϕ, both shown in Fig. 2, which depicts the reflector-antenna geometry with an arbitrarily located strut positioned

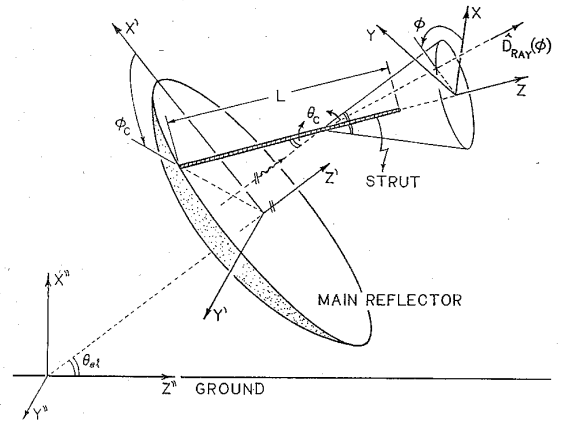

Fig. 2. Strut orientation with respect to the antenna main reflector and ground.

by the angles θ_c and ϕ_c. Using (3) and (4), the radiation-cone contribution to the antenna noise temperature can be written as

$$T(\theta_{el}) = \frac{L\,\rho\,\sin\theta_c}{P_{in}} \int_0^{2\pi} S_s(\vec{\rho})\; T_e(\theta_{el},\phi)\; d\phi\,. \quad (5)$$

Recalling that a reflector antenna normally operates over a range of elevation angles, it is more convenient to consider an average noise-temperature contribution (average value over all elevation angles of operation) given by

$$< T > = \frac{L\,\rho\,\sin\theta_c}{P_{in}} \int_0^{2\pi} S_s(\vec{\rho})\; W_T(\phi)\; d\phi \quad (6)$$

where the average environment noise temperature $W_T(\phi)$ toward a ϕ-direction is given by

$$W_T(\phi) = \frac{1}{\theta_{max} - \theta_{min}} \int_{\theta_{min}}^{\theta_{max}} T_e(\theta_{el},\phi)\; d\theta_{el} \quad (7)$$

and θ_{max} and θ_{min} are the maximum and minimum values of the antenna elevation angle θ_{el}, respectively.

III. Strut Cross-Section Optimization

It is clearly shown in (6) that for a typical environment with a warm ground and a relatively cold sky, a reduction of the strut-cone contribution to the antenna noise temperature can be achieved by reducing the power densities $S_s^{E,H}(\vec{\rho})$ scattered toward the ground. To accomplish this, one must first determine the ϕ-directions where the strut cone illuminates the ground. This can be done considering, once again, Fig. 2. Transforming the scattered-ray direction $\hat{D}_{\mathrm{RAY}}(\phi)$ from the strut local Cartesian coordinate system x, y, z to the x'', y'', z'' coordinate system based on ground, the scattered ray will illuminate the ground whenever $x''_{\mathrm{RAY}}(\phi) \leq 0$. Note that if the angle θ_c is greater than about 45° (the exact value depends on the main-reflector curvature and strut-attachment point), part of the strut cone may strike the main reflector surface. However, in this work it is assumed that θ_c is sufficiently small for this not to occur—mechanically-large reflector antennas generally satisfy this requirement. Also note that the feed and subreflector (if present) will obstruct part of the strut cone. However, since their relative dimensions are usually small, the corresponding effects are also neglected here.

To minimize $<T>$ numerically, it is convenient to approximate (6) by

$$< T > \approx \frac{L\,\rho\,\sin\theta_c}{P_{in}}\; \frac{2\pi}{N_\phi} \sum_{\ell=1}^{N_\phi} S_s(\phi_\ell)\; W_T(\phi_\ell) \quad (8)$$

where $\phi_\ell = 2\pi\ell/N_\phi$ and N_ϕ is the total number of equidistant ϕ-angles used to evaluate the integral. Now, recalling that the sky equivalent noise-temperature ($T_e = T_{sky} \approx 5$ K) is much smaller than the one of the ground ($T_e = T_{grd} \approx 300$ K), (7) can be approximated by

$$W_T(\phi) \approx \frac{\theta_{grd}(\phi) - \theta_{min}}{\theta_{max} - \theta_{min}}\; T_{grd} \quad (9)$$

where $\theta_{grd}(\phi)$ is the value of the elevation angle θ_{el} for which $x''_{\mathrm{RAY}}(\phi) = 0$. It will be assumed here that the antenna operates over the elevation angles $\theta_{max} = 90°$ and $\theta_{min} = 0°$. With the above results, a convenient objective function to minimize the strut-cone noise-temperature contribution can now be constructed using (8) and (9) combined with appropriate penalties. In the present work, the objective function

$$F_{obj} = \sum_{\ell=1}^{N_\phi} \left\{ \frac{W_T(\phi_\ell)}{T_{grd}} \left[W_E\; S_s^E(\phi_\ell) + W_H\; S_s^H(\phi_\ell) \right] \frac{\rho}{\lambda} \right\} + W_{PF}\; F_{pnt} \quad (10)$$

has been used, where S_s^E and S_s^H are given by (1) and (2), respectively, the term ρ/λ has been added to remove the irrelevant ρ-dependence from the scattered cylindrical-wave power density expression, W_E and W_H are weights appropriately chosen to stress the relevance of any particular polarization of interest, and W_{PF} is a weight associated with the soft penalty function F_{pnt}. The soft penalty function F_{pnt} has been added to (10) to impose physical constraints on the cross-section geometry and depends on the particular strut cross-section representation employed, as will be shown. It is important to notice that the average environment noise temperature $W_T(\phi)$ is larger in the ϕ_ℓ-directions that most strongly contribute to the strut-cone noise (i.e., it stresses the directions toward which the strut scattered energy should be minimized).

As mentioned previously, in the inverted-Y strut tripod geometry the top strut generates the strut cone with the dominant ground illumination. This can be readily seen considering Fig. 3, which shows a front view of the reflector antenna with three struts located at $\phi_c = 0°$, 120°, and 240° (the inverted-Y configuration) and their respective strut-cone peak contours (the spherical coordinates θ' and ϕ' are associated with the x', y', z' Cartesian coordinate system of Fig. 2, in the usual form). In this figure, the horizon (border between ground and sky) is also represented for different values of θ_{el} (dashed line). The strut-cone contours located below the corresponding horizon line are directed toward ground. Fig. 3 then clearly shows that the largest strut-cone noise contribution is indeed produced by the top strut ($\phi_c = 0°$). It can also be observed that this noise contribution decreases as the elevation angle

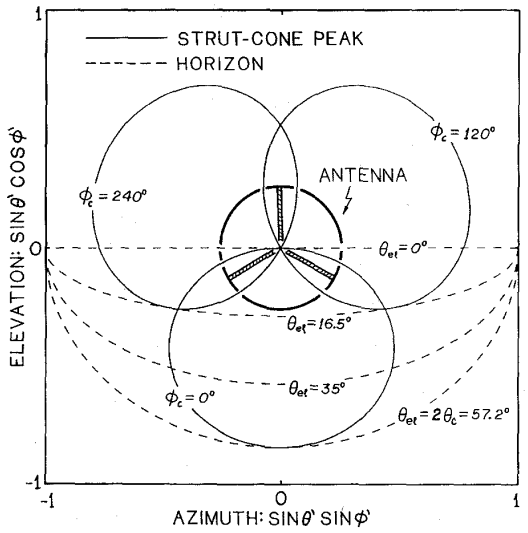

Fig. 3. Strut-cone peak contours for $\theta_c = 28.6°$.

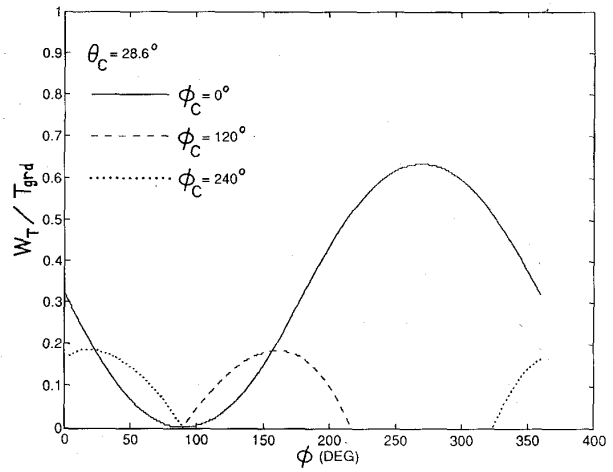

Fig. 4. Average environment noise temperature.

θ_{el} increases. In fact, when $\theta_{el} > 2\theta_c$, the noise contribution considered in this work is not present since only the plane-wave scattering is taken into account. The part of the strut cone that will fall on the ground as the antenna sweeps over its elevation angles of operation is proportional to the average environment noise temperature $W_T(\phi)$ [given by (7)]. Fig. 4 depicts $W_T(\phi)$ as a function of the angle ϕ for each of the three struts of a typical inverted-Y tripod with $\theta_c = 28.6°$. As expected, the top-strut radiation cone illuminates ground more intensely than the other two, and its largest noise contribution comes from the backscattering region ($\phi \approx 270°$). Hence, the minimization of the top-strut noise contribution requires the minimization of its backscattering, and this is accomplished using (10) to optimize the strut cross-section geometry.

In the optimization procedure, the top-strut cross-section contour has been approximated by straight-line segments connecting N_{opt} points with corresponding polar coordinates ρ_i and ϕ_i (see Fig. 5). Each one of these segments is further subdivided by the MoM solution procedure, which requires segments smaller than about 0.2 λ for good accuracy. To reduce the number of variables to be optimized, the ϕ_i coordinates have been kept fixed and only the radial distances ρ_i have been adjusted. This yields N_{opt} unknown values of ρ_i to be determined. Size constraints are imposed using a penalty function F_{pnt} to require that $\rho_{min} < \rho_i < \rho_{max}$ (see Fig. 5). This type of constraint is convenient since it is simple and can be used to indirectly set mechanical strength and cost limits. The specific form of F_{pnt} used here is

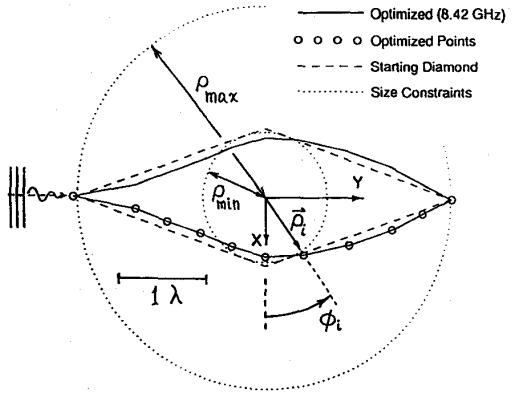

Fig. 5. Cross-section geometries of the starting diamond and optimized strut.

$$F_{pnt} = \sum_{i=1}^{N_{opt}} F(\rho_i) \tag{11}$$

where

$$F(\rho_i) = \begin{cases} (\rho_i - \rho_{min})^2, & \text{if } \rho_i < \rho_{min} \\ (\rho_i - \rho_{max})^2, & \text{if } \rho_i > \rho_{max} \\ 0, & \text{if } \rho_{min} \le \rho_i \le \rho_{max} \end{cases} . \tag{12}$$

Before proceeding toward optimizing specific strut cross sections, consider Fig. 6 which depicts representative scattered power densities of (infinite-length) commonly used struts. The particular results shown correspond to circular (diameter equal to 5.08 cm) and rectangular ($\hat{x}$- and $\hat{y}$-sides equal to 1.33 and 15.24 cm, respectively) cross sections, at an operation frequency of 8.42 GHz (X-band). Circular and rectangular cross sections are commonly used in practice, and the two above were chosen with the same cross-section area (yielding comparable mechanical rigidity). Although these are not optimum cross-section results, they have been included here to provide a reference against which the performance of the optimized strut can be compared. A better strut cross section, from a noise contribution standpoint, is the diamond. Fig. 6 also shows its scattering, for a diamond with diagonals equal to 5.08 and 15.24 cm (comparable to the circular and rectangular cross-section dimensions). The geometries of these three cross sections are shown at Fig. 6(a). Note that for comparable mechanical rigidity, the diamond cross section produces considerably less backscattering radiation, indicating that it has a smaller strut-cone noise contribution than either the circular and rectangular cross sections.

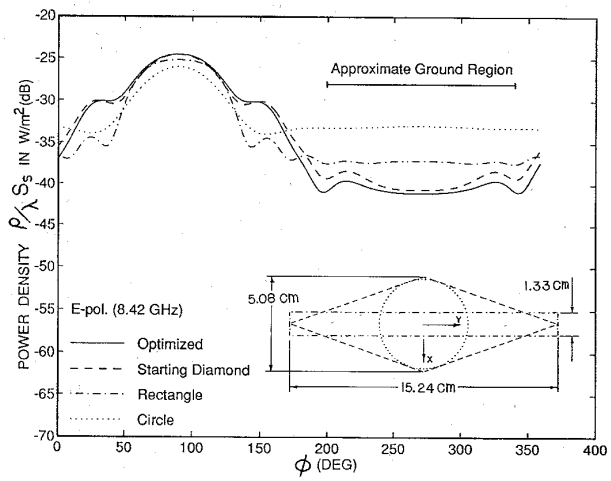

(a)

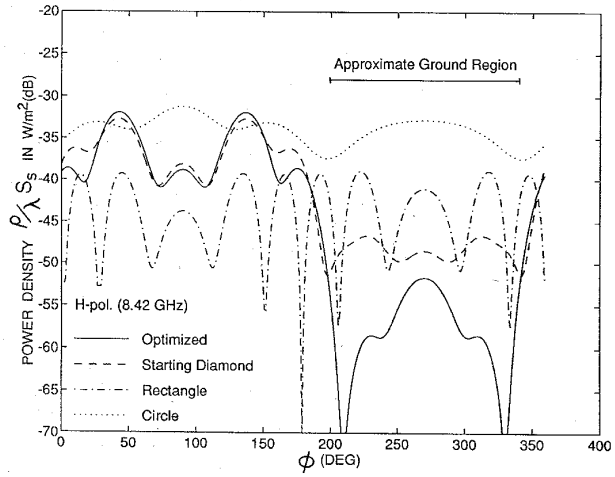

(b)

Fig. 6. Scattering characteristics of infinite-length struts with optimized, diamond, rectangular, and circular cross sections at 8.42 GHz: (a) E-polarization and (b) H-polarization.

Returning to the optimization of the top-strut cross section, the ρ_i values of the previously described diamond shape have been used as the starting point for the numerical procedure. Exploiting the symmetry about the $x = 0$ plane, half of the cross-section contour has been represented by 10 straight-line segments (see Fig. 5), yielding 11 ρ_i-values to be optimized ($N_{opt} = 11$). The weights of (10) have been selected as $W_E = W_H = W_{PF} = 1$ (stressing equally both polarizations), with $W_T(\phi_\ell)/T_{grd}$ given by Fig. 4 (plot with $\phi_c = 0°$). $N_\phi = 360$ equally spaced azimuthal ϕ-directions have been used. The constraints for the optimization variables ρ_i have been selected as $\rho_{min} = 2.54$ cm and $\rho_{max} = 7.62$ cm (equal to half the dimensions of the starting-point diamond diagonals). The optimum cross section obtained is depicted in Fig. 5, and Fig. 6 depicts the corresponding scattering results. The improved backscattering levels are evident, particularly for the H-polarization. These results are typical of the many cases considered in the present work.

IV. Tear-Drop Representation for the Top-Strut Cross Section

In all the optimization runs performed, it was observed that the optimized strut cross section has a shape that resembles a tear-drop (e.g., see Fig. 5). This fact can then be exploited to reduce the computational effort required to optimize the many variables needed to describe the strut by segments. The following closed-form expression is here suggested to represent the tear-drop cross-section contour (see Fig. 7)

$$x(y) = \pm A_m \left\{ \sin\left[\xi + \eta_1 \frac{y}{W_1} + \eta_2 \left(\frac{y}{W_1} \right)^2 \right] - \sin \xi \right\} \tag{13}$$

where W_1 is the strut cross-section width along the $\hat{y}$-direction (assumed given) and A_m, ξ, η_1, and η_2 are parameters that control the cross-section shape—the desired tear-drop shape is obtained with

$$\eta_1 > 0 \quad \text{and} \quad \eta_2 > 0. \tag{14}$$

Although (13) has four parameters, only η_1 and η_2 are independent. Recalling that the cross-section contour must be closed, $x(0) = x(W_1) = 0$. Since $x(0)$ is already equal to zero, to make $x(W_1) = 0$, one then must have

$$\xi = \frac{\pi}{2} - \left(\frac{\eta_1 + \eta_2}{2} \right). \tag{15}$$

The parameter A_m can be obtained from the derivative of (13)

$$\frac{dx}{dy} = \pm \frac{A_m}{W_1} \left(\eta_1 + 2\,\eta_2 \frac{y}{W_1} \right) \times \cos\left[\xi + \eta_1 \frac{y}{W_1} + \eta_2 \left(\frac{y}{W_1} \right)^2 \right] \tag{16}$$

recalling that at the point $y = y_m$, the coordinate x has its extreme values $x_m = \pm W_2/2$, where W_2 is the strut cross-section width along the $\hat{x}$-direction (also assumed given). An expression for y_m can then be derived by equating (16) to zero and solving for y to obtain

$$y_m = \frac{W_1}{2} \left[\sqrt{\left(\frac{\eta_1}{\eta_2} + 1 \right)^2 + 1} - \frac{\eta_1}{\eta_2} \right] \tag{17}$$

where the results from (14) and (15) were used. The substitution of x_m and y_m in (13) yields the desired A_m expression

$$A_m = \frac{W_2}{2} \left\{ \sin\left[\xi + \eta_1 \frac{y_m}{W_1} + \eta_2 \left(\frac{y_m}{W_1} \right)^2 \right] - \sin \xi \right\}^{-1}. \tag{18}$$

Observing that ξ and A_m are given by (15) and (18), respectively, it is clear that, once W_1 and W_2 are specified for a given strut mechanical rigidity, only η_1 and η_2 remain to be determined to fully define the contour. This is done using the optimization procedure described in Section III, together with four appropriate constraints. Two constraints are already given

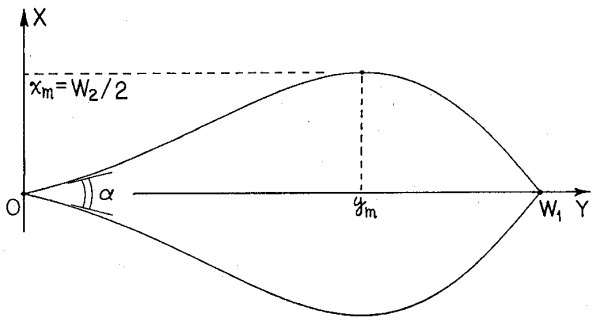

Fig. 7. Tear-drop strut cross section.

by (14). Another is obtained enforcing the fact that the tear-drop contour has only one maximum width W_2 (see Fig. 7) which implies that there is only one y-value where $dx/dy = 0$, namely y_m. From (16), this requires that

$$\xi + \eta_1 \frac{y}{W_1} + \eta_2 \left(\frac{y}{W_1}\right)^2 < \frac{3\pi}{2} \tag{19}$$

which, using (15), yields

$$\eta_1 + \eta_2 < 2\pi. \tag{20}$$

The last constraint is provided by imposing a minimum value α_{min} for the attack angle α, shown in Fig. 7. This avoids a strut with a very sharp edge, which is difficult to manufacture. Recalling that $\tan(\alpha/2) = dx/dy|_{y=0}$, one can write from (15) and (16)

$$\alpha = 2 \arctan\left[\frac{A_m \eta_1}{W_1} \sin\left(\frac{\eta_1 + \eta_2}{2}\right)\right] > \alpha_{min}. \tag{21}$$

The above four constraints can be used to construct the penalty function F_{pnt} of (10). A convenient F_{pnt} for the tear-drop cross section is

$$F_{pnt} = \epsilon_1 \eta_1^2 + \epsilon_2 \eta_2^2 + \epsilon_3 (\eta_1 + \eta_2 - 2\pi)^2 + \epsilon_4 (\alpha - \alpha_{min})^2 \tag{22}$$

where ϵ_1, ϵ_2, ϵ_3, and ϵ_4 are set equal to zero whenever (14), (20), and (21), respectively, are satisfied. Otherwise, they are set to 1.

Using (10), (13), and (22), the variables η_1 and η_2 of the tear-drop cross-section contour have been optimized for the same antenna geometry and operating frequency of Section III. Note that in this case $N_{opt} = 2$, imposing a relatively small computational burden in the numerical optimization procedure. The cross-section widths were set to $W_1 = 15.24$ cm and $W_2 = 5.08$ cm—values that produce strut dimensions comparable to the ones of Section III. The minimum attack angle α_{min} was set to 18.9° (the same attack angle of the triangular cross section defined below). The numerical optimization procedure yielded $\eta_1 = 1.01$ and $\eta_2 = 2.15$.

The optimum tear-drop cross-section contour obtained is depicted in Fig. 8(a), together with two other potentially useful low-noise cross sections. These cross sections are the diamond used as the starting geometry in Section III, and an isosceles triangle with height W_1 and basis W_2. The scattering of the corresponding infinite-length struts is shown in Fig. 8. The relative top-strut noise improvements, computed using (5), are shown on Table I, where T_{td}, T_d, T_t, T_r, and T_c are the strut-cone noise-temperature contributions for the tear-drop, diamond, triangular, rectangular, and circular strut cross sections, respectively (where the rectangular and circular ones are those previously used in Section III). From Fig. 8 and Table I (at 8.42 GHz) we observe that the improvement produced by the tear-drop, relative to the diamond and triangular cross sections, is small for the E-polarization ($T_{td}/T_d \approx 0.83$ and $T_{td}/T_t \approx 0.99$), but more significant for the H-polarization ($T_{td}/T_d \approx 0.40$ and $T_{td}/T_t \approx 0.20$). Also, the diamond, triangular, and tear-drop cross sections have a much smaller noise contribution with respect to the rectangular and circular ones for both polarizations. However, the impact of these improvements on the top-strut noise contribution must take into account the polarization of the reflector-radiated wave and the operating frequency, as well as the antenna elevation angle. For instance, at 8.42 GHz and for a circularly polarized radiation (which has equal amounts of E- and H-polarizations), the improvement produced by the tear-drop over the diamond or triangular cross sections may not be relevant. The reason is that the H-polarization backscattering levels are smaller than the E-polarization ones by approximately 10 and 7 dB, for the diamond and triangle, respectively (see Fig. 8). Hence, any improvement in the top-strut noise contribution is dominated by the reduction of the E-polarization backscattering, which is small [see Fig. 8(a)]. In this particular case, the H-polarization noise pickup can be neglected. Also, if the antenna elevation angle θ_{el} is sufficiently large so that the strut cone does not illuminate the ground, no improvement in the noise temperature associated with the plane-wave scattering is obtained.

Although it is not the objective of this work to study the influence of the strut cross section on the antenna efficiency, we can observe from Fig. 8 that for the E-polarization, the strut scattering toward the antenna boresight ($\phi = 90°$) is practically independent on the cross-section. For the H-polarization, the tear-drop forward scattering is about 5 dB smaller than the triangular one and 2 dB higher than the diamond. However, similarly to the backscattering case, the dominant forward-scattering contribution comes from the E-polarization, and these differences may not be relevant.

One additional advantage of the optimized tear-drop cross section is that its backscattering levels (and, hence, its associated noise-temperature contribution) have a relatively small frequency dependence. This is a consequence of the fact that the tear-drop behavior is not dependent on band-limited effects as may be the case, for example, of corrugated-surface [8] or dielectric-coated struts [9], [10]. This is demonstrated in Fig. 9, which depicts the frequency dependence of the backscattered peak level (over the pattern region $220° \leq \phi \leq 320°$) of the three cross sections shown in Fig. 8(a)—the plots have jagged lines because only a few discrete frequencies have been considered. As evident, the optimized tear-drop scattering is very low and broadband ($S_s \rho/\lambda \approx -40$ dB and -52 dB for the E- and H-polarizations, respectively, from 4 GHz to 40 GHz). In comparison, the corresponding H-polarized backscattering peaks of the diamond and triangular cross sections increase with frequency, reaching levels equal

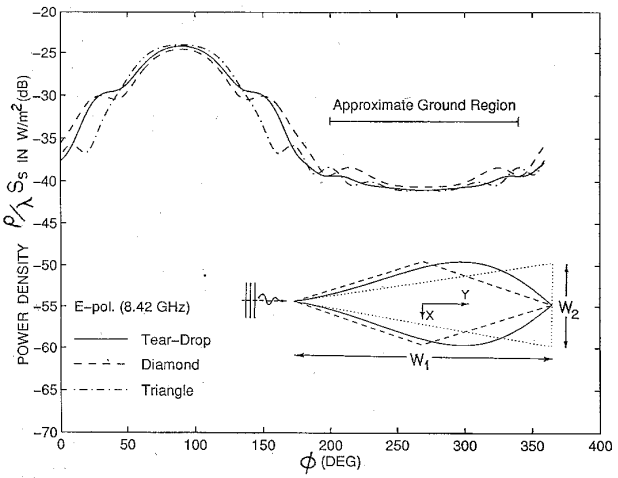

Fig. 8. Scattering characteristics of infinite-length struts with optimized tear-drop, diamond, and triangular cross sections at 8.42 GHz: (a) E-polarization and (b) H-polarization.

TABLE I
NOISE-TEMPERATURE RATIO BETWEEN THE OPTIMIZED TEAR-DROP (T_{td}) AND THE RECTANGULAR (T_r), CIRCULAR (T_c), DIAMOND (T_d), AND TRIANGULAR (T_t) CROSS SECTIONS AT 8.42 GHz AND 31.9 GHz

Freq.	Polariz.	θ_{el}	T_{td}/T_r	T_{td}/T_c	T_{td}/T_d	T_{td}/T_t
8.42 GHz	E-pol.	50°	0.450	0.171	0.886	1.001
		30°	0.525	0.205	0.841	0.995
		10°	0.532	0.209	0.829	0.993
8.42 GHz	H-pol.	50°	0.071	0.007	0.220	0.111
		30°	0.135	0.022	0.402	0.177
		10°	0.164	0.027	0.411	0.201
31.9 GHz	E-pol.	50°	0.093	0.053	0.941	1.073
		30°	0.168	0.067	0.885	1.062
		10°	0.174	0.068	0.871	1.057
31.9 GHz	H-pol.	50°	0.002	0.001	0.056	0.024
		30°	0.006	0.003	0.096	0.041
		10°	0.006	0.003	0.089	0.039

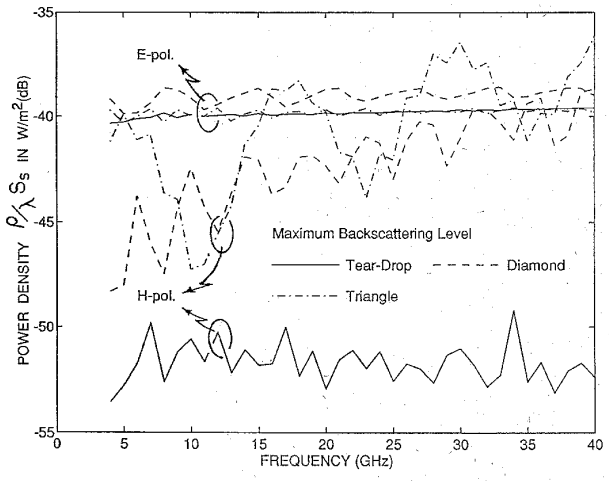

Fig. 9. Frequency dependence of the strut backscattering peak level, over the angular range $220° \leq \phi \leq 320°$, for infinite-length struts with optimized tear-drop, diamond, and triangular cross sections.

or higher than the ones of the E-polarization. These facts indicate that for struts designed to operate over a wide band, at higher frequencies the optimum tear-drop cross section is very effective in reducing the noise associated with the H-polarization. This is exemplified in Table I for 31.9 GHz (Ka-band). From this table, we observe that for the H-polarization, the noise-temperature ratios are $T_{td}/T_d \approx 0.09$ and $T_{td}/T_t \approx 0.04$. However, for the E-polarization the ratios are approximately equal to the unity. For the rectangular and circular cross sections, the T_{td}/T_r and T_{td}/T_c noise ratios are almost zero for both polarizations. These results show that, for a circularly polarized radiation, high frequencies (so that both E- and H-polarizations have comparable backscattering levels), and small elevation angles, the tear-drop cross section is able to suppress the H-polarization backscattering and, consequently, reduce by half the studied top-strut contribution to the antenna noise temperature.

V. CONCLUSION

In reflector-antenna applications, the reduction of the thermal noise associated with the antenna spillover and the plane- and spherical-wave scattering by the struts is of great interest. This work presented a method for optimizing the cross section of reflector-antenna supporting struts to minimize the ground-noise pickup associated with their plane-wave scattering mechanism. It was shown that the struts attached to the main-reflector lower half pick up less plane-wave-scattering ground noise than the ones attached to the upper half. The inverted-Y strut tripod, with its single strut in the reflector top half, is then an optimum configuration to minimize this noise mechanism and, hence, was considered in detail. Since the inverted-Y top-strut noise contribution is much larger than the ones of the other two struts, only the cross section of the top strut was optimized to reduce noise contribution. Numerical optimizations produced a top-strut

cross section with a tear-drop shape, and advantage was taken of this fact to derive a convenient closed-form representation for the optimum cross section.

Representative results were computed for the fields scattered by the tear-drop and other potentially useful strut cross sections (i.e., circle, rectangle, diamond, and triangle). They show that the tear-drop, diamond, and triangle can greatly reduce the plane-wave-scattering ground-noise pickup of antennas employing circular and rectangular struts. When compared with the high performance diamond and triangle cross sections, the tear-drop still can significantly reduce the ground-noise pickup associated with the H-polarization (strut in the plane of the magnetic field), but yields an insignificant improvement for the E-polarization (strut in the plane of the electric field). The advantage of the tear-drop in this case is that as opposed to the diamond and triangle, which have E- and H-polarization noise contributions of the same order when their cross-section perimeters become larger than about 15 wavelengths, the tear-drop maintains a very low H-polarization noise pickup, regardless of its perimeter (broadband performance).

In conclusion, the results obtained show that depending on the existing strut geometry and antenna elevation angles of interest, an optimum cross-section strut can significantly reduce the strut-cone contribution to the noise temperature of reflector antennas.

REFERENCES

[1] W. V. T. Rusch, "Applications of two-dimensional integral-equation theory to reflector-antenna analysis," Tech. Memo. 33-478, Jet Propulsion Lab., May 1971.

[2] W. V. T. Rusch, O. Sørensen, and J. W. M. Baars, "Radiation cones from feed-support struts of symmetric paraboloidal antennas," *IEEE Trans. Antennas Propagat.*, vol. AP-30, pp. 786–790, July 1982.

[3] P.-S. Kildal, E. Olsen, and J. A. Aas, "Losses, sidelobes, and cross polarization caused by feed-support struts in reflector antennas: Design curves," *IEEE Trans. Antennas Propagat.*, vol. 36, pp. 182–190, Feb. 1988.

[4] T. L. Landecker, M. D. Anderson, D. Routledge, R. J. Smegal, P. Trikha, and J. F. Vaneldik, "Ground radiation scattered from feed support struts: A significant source of noise in paraboloidal antennas," *Radio Sci.*, vol. 26, no. 2, pp. 363–373, Mar. 1991.

[5] K. M. Lambert and R. C. Rudduck, "Calculation and verification of antenna temperature for earth-based reflector antennas," *Radio Sci.*, vol. 27, no. 1, pp. 23–30, Jan. 1992.

[6] C. R. Lawrence, T. Herbig, and A. C. S. Readhead, "Reduction of ground spillover in the Owens Valley 5.5-m telescope," *Proc. IEEE,* vol. 82, pp. 763–767, May 1994.

[7] F. J. S. Moreira and A. Prata, Jr., "Optimum strut cross sections for reflector antenna applications," Tech. Rep. 9960-575, Jet Propulsion Lab., Nov. 1995.

[8] T. Satoh, S. Endo, N. Matsunaka, S. Betsudan, T. Katagi, and T. Ebisui, "Sidelobe level reduction by improvement of strut shape," *IEEE Trans. Antennas Propagat.*, vol. AP-32, pp. 698–705, July 1984.

[9] P.-S. Kildal, C. Luptovicz, and O. Forslund, "Hard struts reduce aperture blockage in axisymmetric reflector antennas," in *IEEE Antennas Propagat. Soc. Int. Symp. Dig.*Chicago, IL, June 1992, pp. 1145–1148.

[10] P.-S. Kildal, A. Kishk, and K. Forooraghi, "Thick solid blockage-free struts realized by using a hard surface," in *IEEE Antennas Propagat. Soc. Int. Symp. Dig.*, Ann Arbor, MI, June 1993, pp. 382–385.

[11] R. F. Harrington, *Field Computation by Moment Methods.* New York: IEEE Press, 1993.

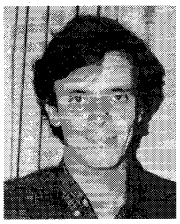

Fernando J. S. Moreira (S'89) was born in Rio de Janeiro, Brazil, on July 18, 1967. He received the B.S. and M.S. degrees in electrical engineering from the Pontificia Universidade Catolica, Rio de Janeiro, Brazil, in 1989 and 1992, respectively. He is currently working toward the Ph.D. degree in electrical engineering at University of Southern California, Los Angeles.

He has authored or coauthored over 10 technical papers in journals and international symposiums. His main interests are applied electromagnetics and numerical techniques for reflector antennas.

Mr. Moreira is a member of Eta Kappa Nu.

Aluizio Prata, Jr. (S'84–M'90) was born on March 18, 1954 in Uberaba, Brazil. He received the B.S.E. degree from the University of Brasilia, Brazil, in 1976, the M.S. degree from the Pontifical Catholic University of Rio de Janeiro, Brazil, in 1979, and the Ph.D. from the University of Southern California, Los Angeles, in 1990, all in electrical engineering. He also holds an M.S.E.E. degree from the California Institute of Technology, Pasadena, 1984.

From 1979–1983, he was with the Telebras Research and Development Center, Brazil, working on the design and construction of satellite earth-station antennas. While at the California Institute of Technology, he designed and implemented one of the first operational neural computers. Currently, he is an Assistant Professor at the University of Southern California, Los Angeles, working with applied electromagnetics. He has been a consultant for several aerospace companies, and has authored or coauthored over 50 articles, patents, and symposium papers.

Dr. Prata is a member of Sigma Xi and Eta Kappa Nu and is currently the Chair of the Los Angeles Chapter of the IEEE Antennas and Propagation Society.

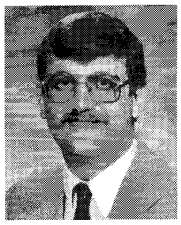

Michael A. Thorburn (S'84–M'86–SM'93) received the M.S. degree in electrical engineering from the University of Southern California, Los Angeles, and the Ph.D. degree in electrical and computer engineering from Oregon State University, Corvallis.

He is the Project Element Manager in the Telecommunications Ground Systems Section at the Jet Propulsion Laboratory in Pasadena, California. Since 1991 he has been involved with the development and refinement of technologies necessary to make Ka-band telecommunications with deep-space efficiency.